A Method for Calculating the Height of Overshooting Convective Cloud Tops Using Satellite-Based IR Imager and *CloudSat* Cloud Profiling Radar Observations

SARAH M. GRIFFIN

Cooperative Institute for Meteorological Satellite Studies, University of Wisconsin–Madison, Madison, Wisconsin

KRISTOPHER M. BEDKA

NASA Langley Research Center, Hampton, Virginia

CHRISTOPHER S. VELDEN

Cooperative Institute for Meteorological Satellite Studies, University of Wisconsin–Madison, Madison, Wisconsin

(Manuscript received 15 June 2015, in final form 17 November 2015)

ABSTRACT

Assigning accurate heights to convective cloud tops that penetrate into the upper troposphere–lower stratosphere (UTLS) region using infrared (IR) satellite imagery has been an unresolved issue for the satellite research community. The height assignment for the tops of optically thick clouds is typically accomplished by matching the observed IR brightness temperature (BT) with a collocated rawinsonde or numerical weather prediction (NWP) profile. However, ''overshooting tops'' (OTs) are typically colder (in BT) than any vertical level in the associated profile, leaving the height of these tops undetermined using this standard approach. A new method is described here for calculating the heights of convectively driven OTs using the characteristic temperature lapse rate of the cloud top as it ascends into the UTLS region. Using 108 MODIS-identified OT events that are directly observed by the *CloudSat* Cloud Profiling Radar (CPR), the MODIS-derived brightness temperature difference (BTD) between the OT and anvil regions can be defined. This BTD is combined with the CPR- and NWP-derived height difference between these two regions to determine the mean lapse rate, $-7.34\,\mathrm{K\,km^{-1}}$, for the 108 events. The anvil height is typically well known, and an automated OT detection algorithm is used to derive BTD, so the lapse rate allows a height to be calculated for any detected OT. An empirical fit between MODIS and geostationary imager IR BT for OTs and anvil regions was performed to enable application of this method to coarser-spatial-resolution geostationary data. Validation indicates that ~75% (65%) of MODIS (geostationary) OT heights are within ±500 m of the coincident CPR-estimated heights.

1. Introduction

Convective storm updrafts that penetrate into the upper troposphere–lower stratosphere (UTLS) region have been recognized and studied using polar-orbiting and geostationary satellite IR and visible channel imagery for several decades. Research has revealed how these ''overshooting top'' (OT) signatures form, as well as their typical duration, microphysical characteristics, and relationships with hazardous weather phenomena (Hung and Smith 1982; Gettelman et al. 2002; Johnson et al. 1994; Dworak et al. 2012). Knowledge of the OT height is especially useful within variety of applications throughout the weather and climate enterprise. OTs serve as a transport mechanism for various atmospheric constituents such as smoke (Fromm and Servranckx 2003), ozone (Pan et al. 2014), and water vapor (Setvák et al. 2008; Wang et al. 2009) and the OT height indicates the altitude to which these constituents are transported. Aviation weather forecasting and hazard avoidance also requires accurate OT height estimates. OTs are associated with strong vertical motion (Mecikalski et al. 2007; Kaplan et al. 2005) and have been linked to convectively

Corresponding author address: Sarah M. Griffin, Cooperative Institute for Meteorological Satellite Studies, 1225 W. Dayton St., Madison, WI 53706.
E-mail: sarah.griffin@ssec.wisc.edu

DOI: 10.1175/JAMC-D-15-0170.1

induced turbulence (CIT) events experienced by aircraft (Bedka et al. 2010). Lane et al. (2003) noted that CIT caused by gravity wave breaking typically occurs about 1 km above an OT. Accurate OT height assignment that is available globally and at high frequency could therefore help better predict where CIT may occur.

Several methods for estimating OT heights have been described in the literature. Radar-derived precipitation echo-top height from sensors such as the ER-2 Doppler radar (Heymsfield et al. 2010), Tropical Rainfall Measuring Mission Precipitation Radar (Zipser et al. 2006), or the *CloudSat* Cloud Profiling Radar (CPR; Luo et al. 2008) as well as ground-based radars such as the WSR-88D (Homeyer and Kumijan 2015) can be used as a proxy for OT height. However, these radar-based methods are limited in their ability to provide continuous coverage necessary for global aviation weather forecasting. Another approach uses visible channel imagery to determine the magnitude of OT penetration above the anvil by measuring the length of shadow produced by the OT (Fujita 1972; Kaňák et al. 2012; Bedka et al. 2015), which can be added to the anvil cloud height to derive an OT height. However, it is limited to daylight hours and an automated method to recognize shadows and compute their length does not yet exist. A stereo-based method has been incorporated within the Multiangle Imaging Spectroradiometer (MISR) top-of-atmosphere cloud data product (Chae and Sherwood 2010) to retrieve deep convective cloud heights, but this method lacks temporal frequency as MISR is on board the polar-orbiting *Terra* satellite.

Given that convective anvil cloud heights derived from IR are generally quite accurate in opaque conditions (Weisz et al. 2007), height assignment for the tops of most optically thick anvil clouds can be accomplished in real time by matching their satellite IR brightness temperature (BT) to the appropriate vertical level within a collocated rawinsonde or numerical model temperature profile. Unfortunately, this method cannot be used to derive OT heights because an OT typically has an IR BT that is colder than any vertical level in the associated profile. No other viable method for real-time OT height assignment has been demonstrated.

This study presents a new method for calculating OT heights using IR satellite data. This method is based upon time-synchronized and geo-collocated observations of OTs from Moderate-Resolution Imaging Spectroradiometer (MODIS) and the *CloudSat* CPR. These datasets are used to define the characteristic lapse rate of OTs as they ascend through the anvil into the UTLS. We will show that the IR BT difference between an OT and the surrounding anvil derived by automated IR-based OT detection algorithms (Bedka et al. 2010; Monette et al. 2012) can be combined with the IR-based estimate of anvil height and the characteristic UTLS lapse rate to derive an OT height that is typically accurate to within 500 m of the CPR-derived height. An empirical fit between 1-km MODIS and 3+-kilometer-spatial-resolution geostationary (GEO) IR BT observations within OT regions is developed, allowing an extension of this approach to any GEO IR imager in near–real time.

The manuscript is organized as follows: sections 2 and 3, respectively, discuss the data and methodology utilized in the research; section 4 presents the results; a method for converting the overshooting heights to pressure altitude coordinates for aviation applications is presented in section 5, and conclusions are given in section 6.

2. Data

OTs and associated anvil cloud properties derived from MODIS and GEO IR imagery by an automated OT detection algorithm and *CloudSat* CPR profiles are the primary datasets used in this study. The MODIS and CPR data are used to compute a mean temperature lapse rate for a large sample of manually verified OT detections that were found along coincident *CloudSat* tracks. MODIS OT properties are compared with collocated and time-matched GEO-derived OT properties to develop a regression that allows the MODIS-based lapse rate to be applied to coarser spatial resolution GEO data. The datasets used in this study are described here, and the methodology for applying these datasets to derive OT heights is described in section 3.

a. Aqua *MODIS satellite imagery*

MODIS granules with known *CloudSat* OT overpasses are processed within automated OT detection algorithms (Bedka et al. 2010; Monette et al. 2012). Please see the methodology section (section 3) for a brief description of the OT detection algorithms. MODIS IR imagery has a 1-km spatial resolution and an equatorial overpass time of 0130/1330 local time MODIS imagery suffers from a "bowtie" effect, where one scan line's leading edge will overlap another scan line's trailing edge along the periphery of the swath (Wolfe et al. 1998). To eliminate any impacts of this effect, only OTs within 150 km of the *Aqua* subsatellite point are utilized in this analysis.

b. GEO satellite imagery

IR observations from two GEO satellite imagers are used in this study: the Meteorological Satellite (Meteosat) Second Generation (MSG) Spinning Enhanced Visible and Infrared Imager (SEVIRI) and the eastern Geostationary Operational Environmental Satellite (GOES-E) imagers. SEVIRI imagery (0°W nadir), which offers 3-km

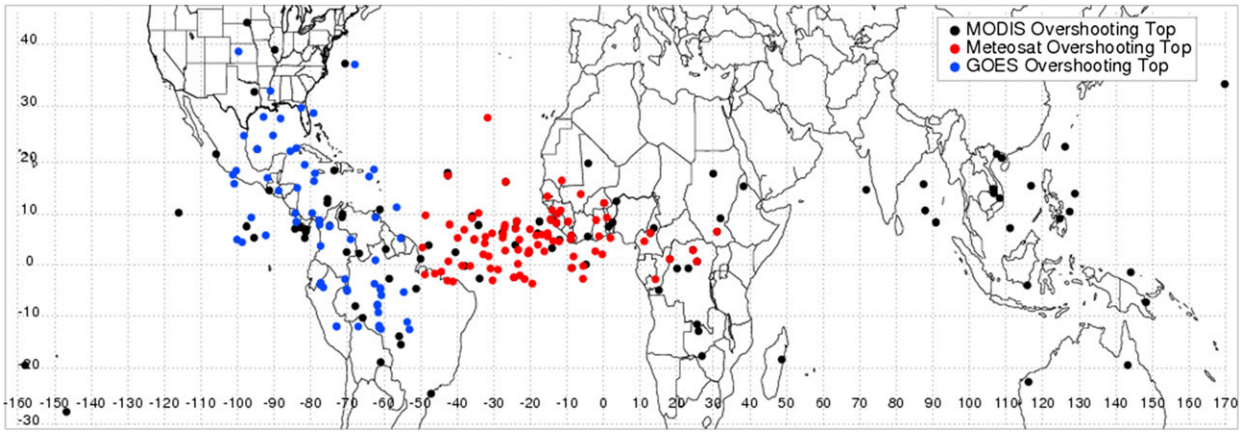

FIG. 1. The location of 108 MODIS, 84 SEVIRI, and 61 GOES OTs that are within 6 km and 5 min of a *CloudSat* overpass. These OTs serve as the dataset used to calculate the OT height.

spatial and 15-min temporal resolution, is utilized between 50°W and 40°E. GOES-E contiguous-U.S. imagery (75°W nadir), which offers 15-min temporal and 4-km spatial resolution, is examined between 110° and 62°W and north of 20°N. OT regions between 50° and 62°W and south of 20°N were identified using a GOES-E Northern Hemisphere scan, which is conducted every 30 min.

In the methodology described below, MODIS and GEO OT detections are collocated to compare OT properties from the two sets of sensors. MODIS and GEO OTs are considered to be collocated if they are within 2.5 min and 5 km of each another. These criteria provided 514 (351) collocated MODIS and SEVIRI (GOES) OT detections between the March 2008 and December 2013 study period.

c. CloudSat *Cloud Profiling Radar*

The *CloudSat* satellite operates within the NASA A-Train constellation and collects observations within 2 min of *Aqua* MODIS. The CPR is an active sensor that emits and detects reflected microwave energy at a frequency (wavelength) of 94 GHz (3.2 mm). The footprint of a *CloudSat* CPR profile covers 1.7 km in the along-track direction and 1.3 km in the across-track direction. A new profile is captured every 1.1 km, indicating that there is some overlap between adjacent profiles (i.e., oversampling). The effective vertical resolution is 480 m, with oversampling at 240-m resolution. The 2B-GEOPROF product provides a cloud mask and radar reflectivity at each of the 125 vertical data bins (Reinke et al. 2009).

MODIS and GEO OTs are collocated with manually identified *CloudSat* OTs to provide a comparison for the OT height assignment. A *CloudSat* OT is visually identified by plotting vertical profiles of CPR reflectivity and looking for 1) a continuous CPR reflectivity extending to approximately the top of the boundary layer and 2) a noticeable abrupt increase in the upper-level extent of CPR reflectivity values greater than or equal to −25 dBZ relative to the CPR reflectivity within an annulus of roughly 0.05° and 0.1° latitude. The imagers and *CloudSat* OT observations are required to be within 6 km and 5 min of each other to be considered a match. With this constraint, 108 MODIS and *CloudSat* OT collocations were found during the study period. In addition, 84 (61) SEVIRI (GOES) and *CloudSat* OT collocations were also found. The location of these OT events can be seen in Fig. 1. Only 10 (4) of the SEVIRI (GOES) OTs correspond with MODIS OTs due to mismatches in GEO and MODIS observation time. *CloudSat* OT locations are parallax-corrected to match the location of MODIS OTs using the method from Wang et al. (2011) while geostationary OTs are also parallax-corrected to the *CloudSat* OT locations.

Given the wavelength of the CPR pulse, the CPR signal often penetrates through the small particles typically present near the cloud top. As a result, the uppermost height of the returned CPR signal will often be below that observed by the *Cloud–Aerosol Lidar and Infrared Pathfinder Satellite Observation* (*CALIPSO*) Cloud–Aerosol Lidar with Orthogonal Polarization (CALIOP) that also operates within the A-Train constellation. However there are several challenges in working with CALIOP data for OT height analysis that are described by Bedka et al. (2012), with the primary challenge being that the CALIOP version-2 cloud-top height product often fails to provide heights in OT regions. Thus, CPR data allow us to best perform the analysis described in this paper.

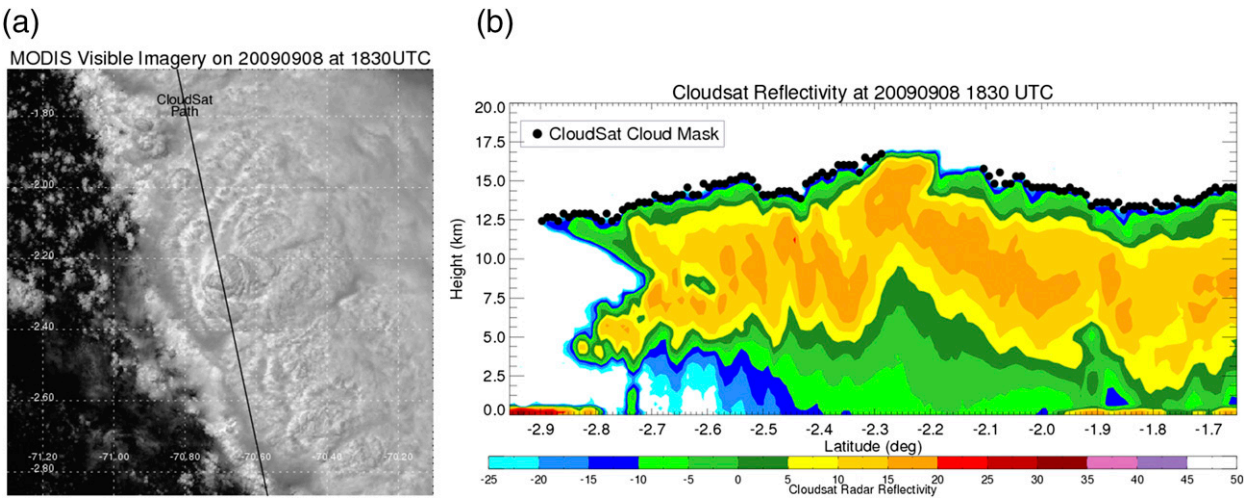

FIG. 2. (a) MODIS 250-m spatial resolution visible imagery and *CloudSat* path over an OT. (b) *CloudSat* Cloud Profiling Radar reflectivity (colored) and cloud mask (circles). Note the lack of cloud mask over the highest −25-dB*Z* CPR reflectivity.

The *CloudSat* cloud-top height is considered to be the height of the highest CPR reflectivity ≥ −25 dB*Z*. Reflectivity is used instead of the provided CPR cloud mask because this product can potentially be unreliable. According to the CloudSat Data Processing Center (2007), a user ''should consider using cloud-mask values of 30,'' which represent a ''good [radar] echo'' with less than 2% false detection. However, while Fig. 2a indicates that the *CloudSat* CPR observed a deep convective cloud, there is no CPR cloud mask ≥30 collocated with the −25-dB*Z* CPR reflectivity in Fig. 2b. Of the 108 MODIS overshoots in this dataset, 3 do not have a corresponding CPR cloud mask. The average of the CPR reflectivity associated with a CPR cloud mask value ≥30 for the remaining 104 MODIS overshoots is −20.74 dB*Z*. We decided to round to −25 dB*Z* because the CPR is potentially not observing the tallest part of the overshoot, and −25 dB*Z* should be a bit higher in the atmosphere than −20.74 dB*Z*.

d. *Numerical weather prediction (NWP) model profiles*

Temperature profiles from the Global Data Assimilation System (GDAS; NCDC 2015) are utilized in combination with satellite-based estimates of anvil cloud IR BT to derive anvil cloud heights. These heights are used in the methodology described below to calculate OT heights. The GDAS analyses have a vertical resolution of 26 pressure levels and 1.0° horizontal resolution. For real-time applications, forecast profiles of temperature and height from virtually any NWP model with comparable or better vertical and spatial resolution could be used to calculate the anvil height.

3. Methodology

a. *Automated satellite-based OT detection*

An objective satellite-based OT detection algorithm (Bedka et al. 2010) and its derivative, the tropical OT detection algorithm (Monette et al. 2012), are used to first identify OTs and derive their respective BT and anvil mean BT. OTs are defined as a ''domelike protrusion above a cumulonimbus anvil, representing the intrusion of an updraft through its equilibrium level,'' according to the American Meteorological Society's *Glossary of Meteorology* (Glickman 2000). These algorithms identify candidate OT regions that have an IR BT colder than 215 K. The mean BT of the anvil cloud surrounding the OT candidates is then computed. Candidate OT pixels that are significantly colder than the surrounding anvil are classified as OTs. The Bedka et al. and Monette et al. approaches use differing detection criteria but are constructed using similar logic. In our study, if the OT IR BT is colder than the tropopause (determined from NWP model temperature profiles), the Bedka et al. method is used to derive the anvil BT. In the Bedka et al. method, 5 of 16 anvil pixels need to be colder than 225 K to calculate the mean anvil BT, and the OT BT needs to be 6.5 K colder than the mean anvil BT. If the OT IR BT is warmer than the tropopause, the Monette et al. method, with more stringent OT anvil thresholds, is employed. This can be common in the tropics, as Liu and Zipser (2005) suggest that the equilibrium level in the tropics is below the tropical tropopause. Here, 9 of 16 anvil pixels need to be colder than 225 K to calculate the mean anvil BT, and the OT BT needs to be 9 K colder than the mean anvil BT. In either

case, the IR BT of each OT pixel, the minimum IR BT within the OT, and the anvil mean BT are recorded. The OT–anvil BT difference and anvil BT are used to derive the local lapse rate described below.

b. MODIS OT height calculation

At this point, we have most of the information necessary to estimate an OT height using the following equation:

$$\text{OT Height} = \text{Anvil Height} + \frac{\text{OT BT} - \text{Anvil BT}}{\text{OT Lapse Rate}}. \quad (1)$$

The anvil height is found by comparing the mean anvil BT derived from the OT detection algorithms above to the GDAS temperature and height profiles to find the best approximation. Vertical interpolation of the GDAS profile is performed to aid in this approximation. If an anvil BT is colder than the NWP tropopause, the anvil height is defined as the tropopause height plus the difference between the anvil BT and the tropopause temperature divided by the moist adiabatic lapse, which is calculated using the method from Randall (2009).

The MODIS-derived anvil cloud height using the GDAS profiles is compared with the *CloudSat* anvil height to assess accuracy of the imager-based calculation. The *CloudSat* anvil height is defined as an average of the two lowest cloud-top heights (based on −25-dBZ reflectivity) along the *CloudSa*t overpass within 8 km of the location of the peak OT height. Since *CloudSat* orbits along a north–south track (Goddard Earth Sciences Data and Information Services Center 2015) with an across-track footprint of 1.3 km, one anvil height is determined from reflectivities to the north of the OT, and the other to south of the OT. The 8-km criterion is used because typical OT signatures have a diameter <15 km (Bedka et al. 2010).

The OT lapse rate needed in Eq. (1) is negative and defined as the OT minimum BT minus anvil BT (both from MODIS) divided by the height difference between the peak *CloudSat* OT height and the associated anvil height derived from the MODIS anvil BT. The OT lapse rate can vary, ranging from −5.0 to −22.5 K km^{-1}. This range can be attributed to issues such as a slightly inaccurate anvil BT calculation, an errant GDAS temperature profile, BT smoothing induced by small OT signatures that do not fill a MODIS IR pixel, and several other second-order effects. Yet, 50% of the lapse rates are between −6.7 and −9.0 K km^{-1}. In addition, there is little correlation (0.124) between the absolute value of the OT latitude and lapse rate, indicating that the OT lapse rates have no latitudinal dependency. Furthermore, the seasonal differences (ignoring outliers) in the observed lapse rates are also small, ranging from −7.8 K km^{-1} for June–August to −7.0 K km^{-1} for December–February. So we will use the median of the 108 MODIS lapse rates, −7.34 K km^{-1}, in Eq. (1) to derive OT height.

Since this study has a relatively small dependent dataset to work with (108 MODIS OTs), a cross-validation approach is utilized to better predict the discrepancies in the calculated OT heights. Cross validation simulates unknown data by repeating procedures on a data subset and then examining on the portions of data left out of the subset (Wilks 2006). In this approach, the dependent dataset of 108 MODIS OTs is divided into two smaller datasets. The first dataset is 30 randomly chosen MODIS OTs; the second dataset is the remaining 78 MODIS OTs. The median lapse rate is calculated from the first dataset and is then used to calculate the OT height for the second dataset. This process is repeated 50 times, resulting in 4000 MODIS OT height calculations. Since we are interested in the percentage of OT heights within a certain range of the CPR height, these 4000 MODIS OT heights will be used to create a probability distribution.

c. GEO imager OT height calculation

Similar to the process used for estimating MODIS OT heights, GEO-based OT heights are calculated using Eq. (1), incorporating the median lapse rate value for the 108 MODIS values of −7.34 K km^{-1}. However, because the GEO imager pixel sizes are coarser than for MODIS (at least 3 times the size), the GEO-observed OT BT observations are biased warmer than those from MODIS. For example, Bedka et al. (2010) reported a 12-K mean BT difference for many OT events observed by MODIS, AVHRR, and *GOES-12*. Hillger et al. (2013) reported a 7-K BT difference between MODIS and *GOES-13* for one OT.

In order for Eq. (1) and the MODIS-based lapse rate to be applicable to the warmer GEO-based OT observations, a linear regression between GEO and MODIS OT and anvil BT observations is calculated to normalize the GEO BTs to MODIS. The linear regressions between the SEVIRI and MODIS anvil and OT BT are

$$\text{MODIS OT BT} = 0.9825(\text{SEVIRI OT BT}) + 0.1265 \quad \text{and} \quad (2)$$

$$\text{MODIS Anvil BT} = 0.9767(\text{SEVIRI Anvil BT}) + 2.439. \quad (3)$$

These equations are the result of a linear regression between 514 collocated SEVIRI and MODIS OTs

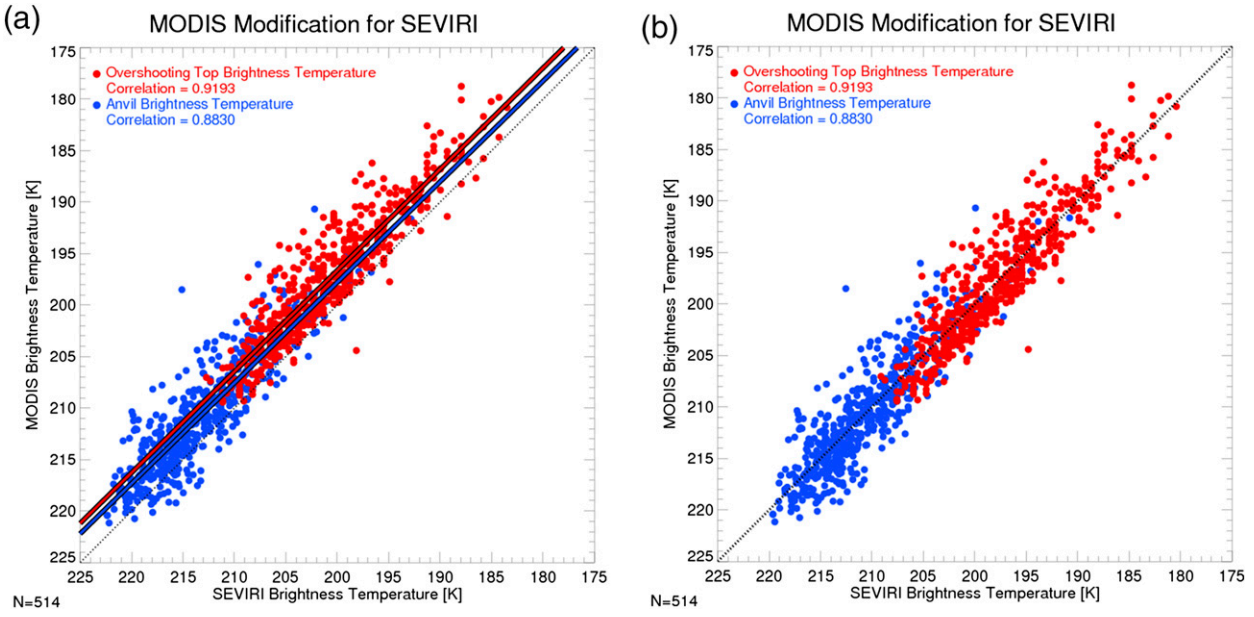

FIG. 3. (a) Comparison between SEVIRI and MODIS anvil and OT brightness temperatures. The red (blue) solid line represents the linear regression equation between MODIS and SEVIRI OT (anvil) BT. (b) Comparison between SEVIRI and MODIS anvil and OT brightness temperatures after the linear regression from Eqs. (2) and (3) are applied to the SEVIRI OTs.

shown in Fig. 3a. Overall, the SEVIRI OT (anvil) BT is about 3 K (2 K) warmer than the corresponding MODIS BT, which is expected given that MODIS has a higher spatial resolution than SEVIRI. The relationship between SEVIRI and MODIS after the linear regressions are applied can be seen in Fig. 3b. The linear regressions between the GOES and MODIS anvil and OT BT are

$$\text{MODIS OT BT} = 0.9713(\text{GOES OT BT}) - 2.3388 \quad \text{and} \tag{4}$$

$$\text{MODIS Anvil BT} = 0.9342(\text{GOES Anvil BT}) + 8.741. \tag{5}$$

These equations are the result of a linear regression between 351 collocated GOES and GOES OTs

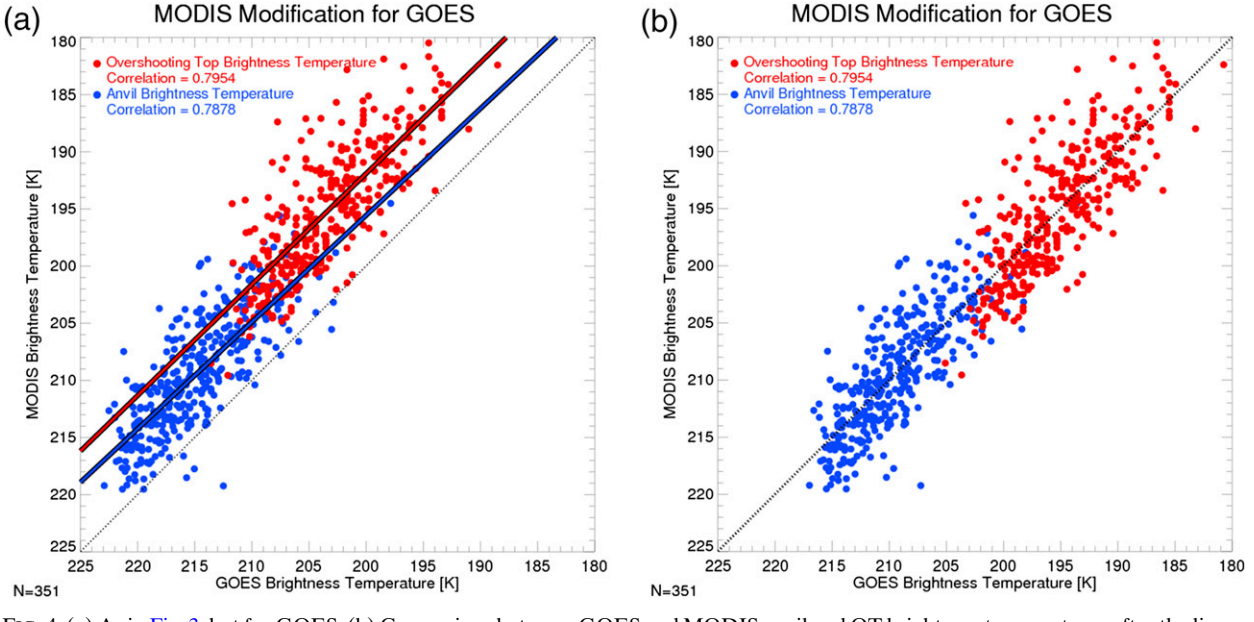

FIG. 4. (a) As in Fig. 3, but for GOES. (b) Comparison between GOES and MODIS anvil and OT brightness temperatures after the linear regression from Eqs. (4) and (5) are applied to the GOES OTs.

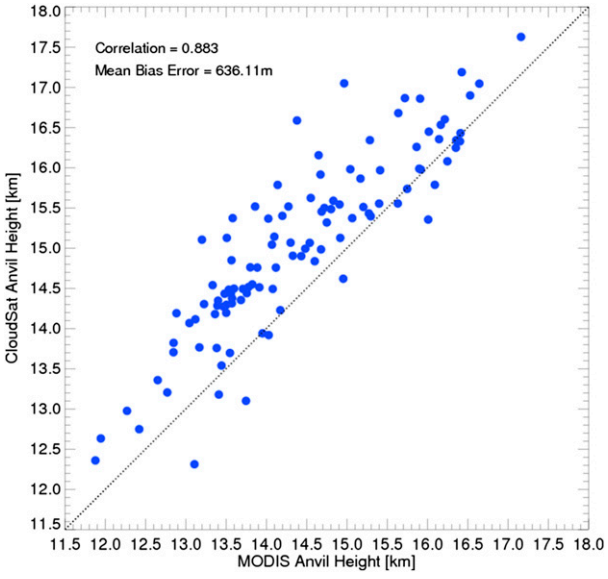

FIG. 5. The relationship between the MODIS anvil height (the height of the MODIS anvil BT in the GDAS profile) and corresponding *CloudSat* anvil heights.

shown in Fig. 4a. The GOES OT (anvil) BT are about 8 K (5 K) warmer than MODIS, which is again expected as MODIS has a higher spatial resolution compared to GOES. These biases are in agreement with Sherwood et al. (2004), who found that 4-km imagery experiences a 5–7-K bias relative to the cloud physics lidar. The relationship between GOES and MODIS after the linear regressions are applied can be seen in Fig. 4b.

The adjusted GEO anvil BT is then compared with the GDAS temperature and height profiles at the OT location to calculate anvil height, with the OT height calculated using Eq. (1) with the adjusted GEO OT BT. The results of using this method to estimate OT heights are given in the next section.

4. Results

a. *MODIS estimates of OT height*

Using the dependent dataset of 108 OTs, we first compare the MODIS anvil height with the *CloudSat* anvil height. Figure 5 shows that the two anvil height estimates have a correlation coefficient of 0.883. Overall, the *CloudSat* anvil height is higher than MODIS, with a mean bias of about 636.11 m. However, this difference will not be an issue in the overall OT height calculation. Since the *CloudSat* anvil height is generally higher than the anvil BT height, the difference is compensated by a slightly smaller lapse rate magnitude, relative to *CloudSat*, in Eq. (1).

For 108 MODIS OTs, the median lapse rate is $-7.34\,\mathrm{K\,km^{-1}}$, which we will use in Eq. (1) to derive the OT height. The MODIS OT height results using this lapse rate are shown in Fig. 6a. However, this is not an accurate representation of OT height accuracy, since the same MODIS OTs are used to both calculate the lapse rate value and the OT height accuracy. So, a cross-validation approach is utilized to predict future OT height difference. The results of this analysis are shown in Fig. 6b. Overall, there is a 50% (75%) probability of MODIS-estimated OT height are within 230 m below and 340 m above (380 m below and 480 m above) the *CloudSat* height. The distribution of heights within 1000 m of the *CloudSat* height is disproportionate with more MODIS OT heights being placed above the *CloudSat* height. However, this is deemed plausible, since *CloudSat* may not have sampled the highest (and therefore coldest) OT pixel observed in MODIS.

Another way to characterize the OT height differences between MODIS and *CloudSat* is to look at the

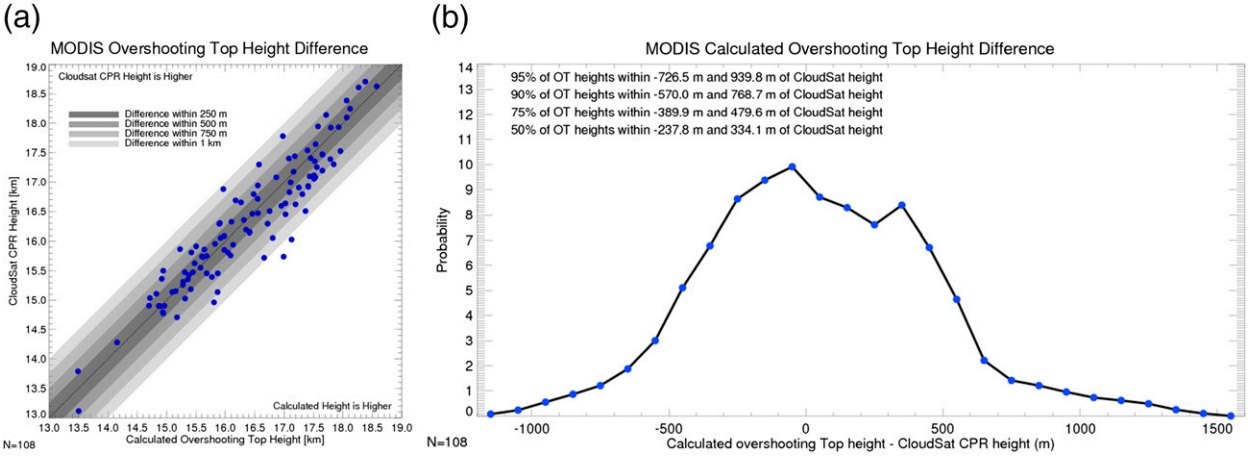

FIG. 6. (a) Calculated OT height difference for MODIS. (b) Distribution of the calculated MODIS OT height differences for the cross-validation experiment. About 75% of the OT are within 500 m of the *CloudSat* cloud height.

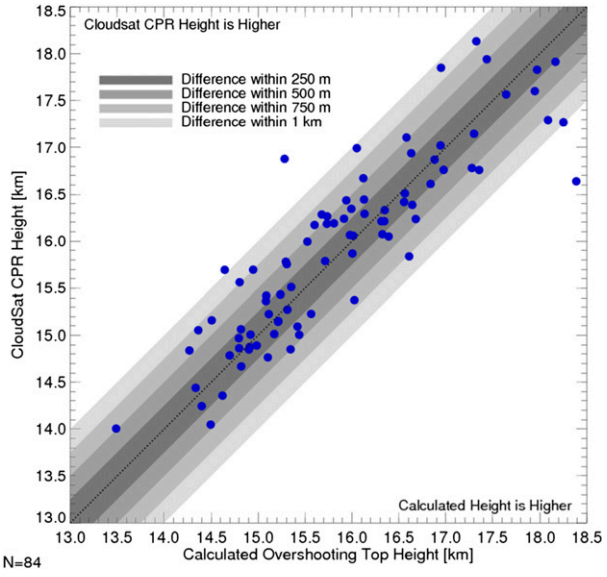

FIG. 7. Comparison between the calculated SEVIRI OT height and the *CloudSat* CPR height.

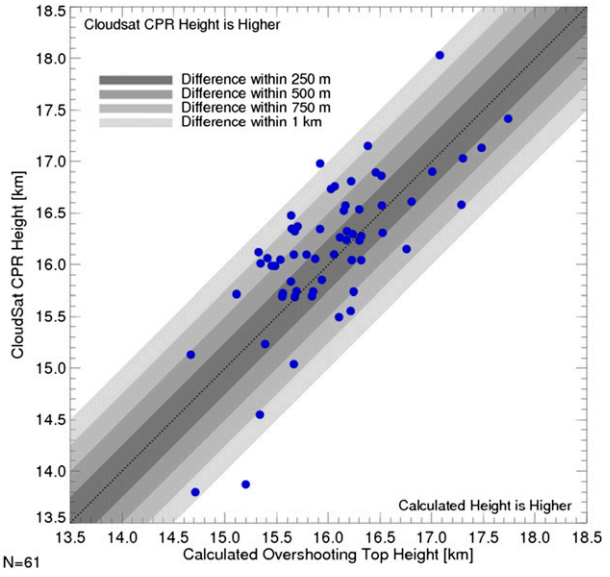

FIG. 8. Comparison between the calculated GOES OT height and the *CloudSat* CPR height.

percentage of overshoot depth, with overshoot depth defined as the difference between the *CloudSat* OT height and the *CloudSat* anvil height. Overall, about 75% of OTs have a height difference between MODIS and *CloudSat* OT heights that is less than or equal to half of the overshoot depth.

b. *SEVIRI estimates of OT height*

Using Eqs. (1)–(3) and a lapse rate of $-7.34\,\mathrm{K\,km^{-1}}$, the height of 84 SEVIRI-identified OTs is calculated and compared with the *CloudSat* height. Observed in Fig. 7, 41.7% (72.6%) of the calculated OT heights are within 250 m (500 m) of the *CloudSat* OT height. *CloudSat* heights are higher than the SEVIRI height by an average of 96.5 m. Overall, only 3 of 84 (3.5%) SEVIRI OTs have a height difference magnitude greater than 1 km. One of these OTs has a calculated height 1751 m above the *CloudSat* height. The cause of this discrepancy may be twofold. First, the OT anvil height is poorly defined. Comparison of the anvil BT with the nearest sounding, which is 580 km away and about 3 h earlier than the OT, indicates that the anvil height may be about 600 m too high. As the OT and sounding are from 0300 and 0000 local standard time, respectively, this difference does not appear to be the result of diurnal variations in convection (Liu and Zipser 2008). Second, *CloudSat* may have missed the highest point of OT. Based on the OT BTD, the characteristic difference between the *CloudSat*-observed OT and anvil heights should be about 1400 m. However, this *CloudSat* observation has a difference of only 1074 m.

c. *GOES estimates of OT height*

Using Eqs. (1), (4), and (5) and a lapse rate of $-7.34\,\mathrm{K\,km^{-1}}$, the height of 61 GOES-identified OTs is calculated and compared with the *CloudSat* height. The results of the GOES–*CloudSat* OT height comparison are shown in Fig. 8. Overall, about 37.7% (57.7%) of the calculated GOES OT heights are within 250 m (500 m) of the *CloudSat* height. *CloudSat* heights are higher than the GOES height by an average of 151 m. Only two (3.3%) GOES OTs have a height difference magnitude greater than 1000 m; however, one OT has a calculated height about 1.33 km above the *CloudSat* height.

The case featuring about a 1.33-km difference highlights one potential weakness in the OT height calculation, namely, the use of NWP model data to calculate the anvil height. Figure 9 shows a comparison between the GDAS analysis used in this study and a 12-h forecast from the 0.5° resolution Global Forecast System (GFS), valid at the same time for this case. Although the profiles look similar at first glance, the GDAS analysis (left panel) shows a tropopause pressure of 91.3 hPa, while the GFS (right panel) shows a tropopause pressure of 166.3 hPa. This discrepancy results in a 700-m difference in anvil height. However, this discrepancy is uncommon, as an analysis of 63 OT events indicates that 61.9% (92.1%) of GFS anvil heights are within ±50 m (±100 m) of the GDAS anvil height (not shown).

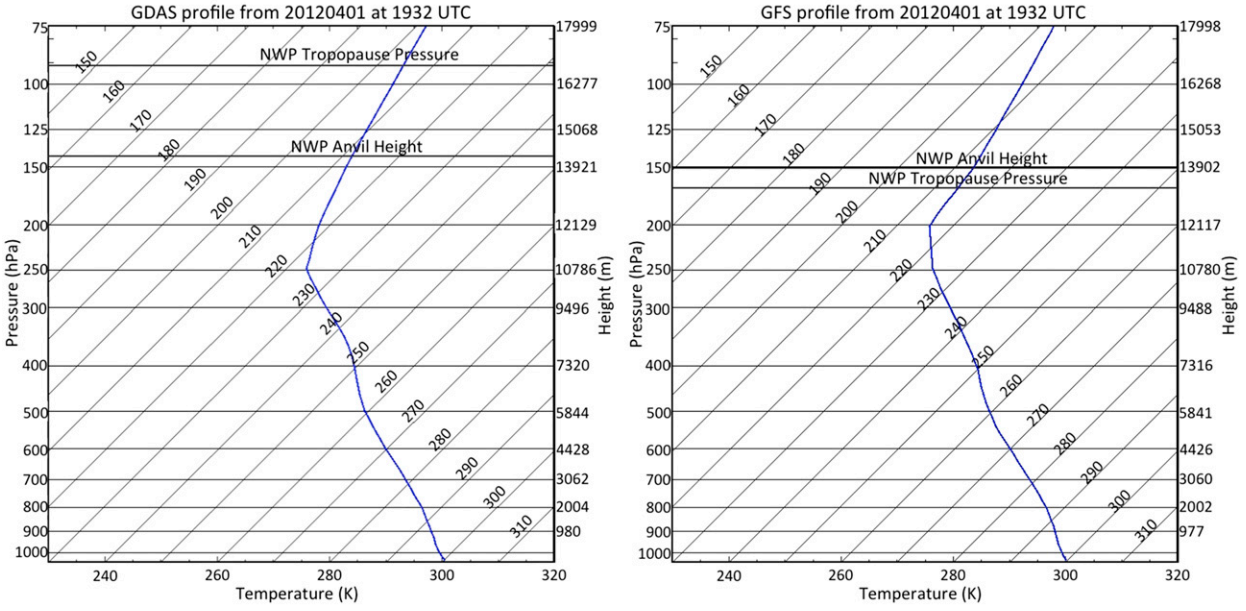

FIG. 9. (left) The GDAS analysis and (right) 12-h GFS temperature profile for a selected OT event, valid at the same time. The 0-h GDAS has a tropopause pressure of 91.3 hPa, and the 12-h GFS has a tropopause pressure of 166.3 hPa.

d. Evaluating accuracy when using the NWP tropopause height as the anvil height

Another potential way of calculating an OT height is by utilizing a collocated NWP-estimated tropopause analysis/forecast height. If the OT anvil height is considered the tropopause height, then the OT height is the OT anvil height plus the distance that the OT extends into the stratosphere. For this method, Eq. (1) can be rewritten as

$$\text{OT Height} = \text{Tropopause Height} + \frac{\text{OT BT} - \text{Tropopause Temperature}}{\text{OT Lapse Rate}}.$$

We can then compare our method of calculating the anvil height using the anvil BT and a GDAS NWP profile of temperature and pressure with the method that assumes the anvil height is the tropopause height. Since the OTs need to extend into the stratosphere to utilize the NWP tropopause height, the OT BT needs to be colder than the NWP tropopause temperature. This restriction reduces the number of OTs for this analysis to 71 MODIS OTs, 44 SEVIRI OTs, and 33 GOES OTs. Using the 71 MODIS OTs, the OT lapse rate is recalculated to $-7.02\,\text{K km}^{-1}$.

The results when using an NWP tropopause height as a proxy for anvil height can be seen in Fig. 10. Overall, a high OT height bias exists when compared with the *CloudSat* CPR heights. For MODIS-identified OTs (Fig. 10a), there is a 75% probability an OT height is between 125 m below and 1118 m above the *CloudSat* CPR height when utilizing the NWP tropopause height as the anvil height. When utilizing the anvil BT to calculate the anvil height, this range is 380 m below and 480 m above. There is only a 48.7% probability that a MODIS OT height is within 380 m below and 480 m above the *CloudSat* CPR height when using the NWP tropopause height. For GEO-identified OTs (Fig. 10b) about 58% have a calculated height higher than the *CloudSat* CPR height, and 9.1% (12.1%) of SEVIRI (GOES) OTs have extreme (>1 km) height differences from the *CloudSat* CPR height, with one GOES-identified OT having a height difference of over 4.5 km. These numbers are much larger than using the anvil BT to calculate the anvil height. Therefore, the method of using NWP-provided tropopause height as the anvil height is much less accurate than using the anvil BT to assess the anvil height when calculating the overall OT height. One potential reason is the NWP tropopause height does not compare well to the *CloudSat* anvil height. When using the MODIS anvil BT to calculate the anvil height, a high correlation (0.883) and fairly consistent bias exists. The GDAS tropopause height, however, only has a correlation of 0.417 with the *CloudSat* anvil height and the bias is much less consistent (Fig. 11).

5. Conversion for aviation applications

Since the OT height calculation relies to some extent on the NWP temperature profiles, OT heights are presented in

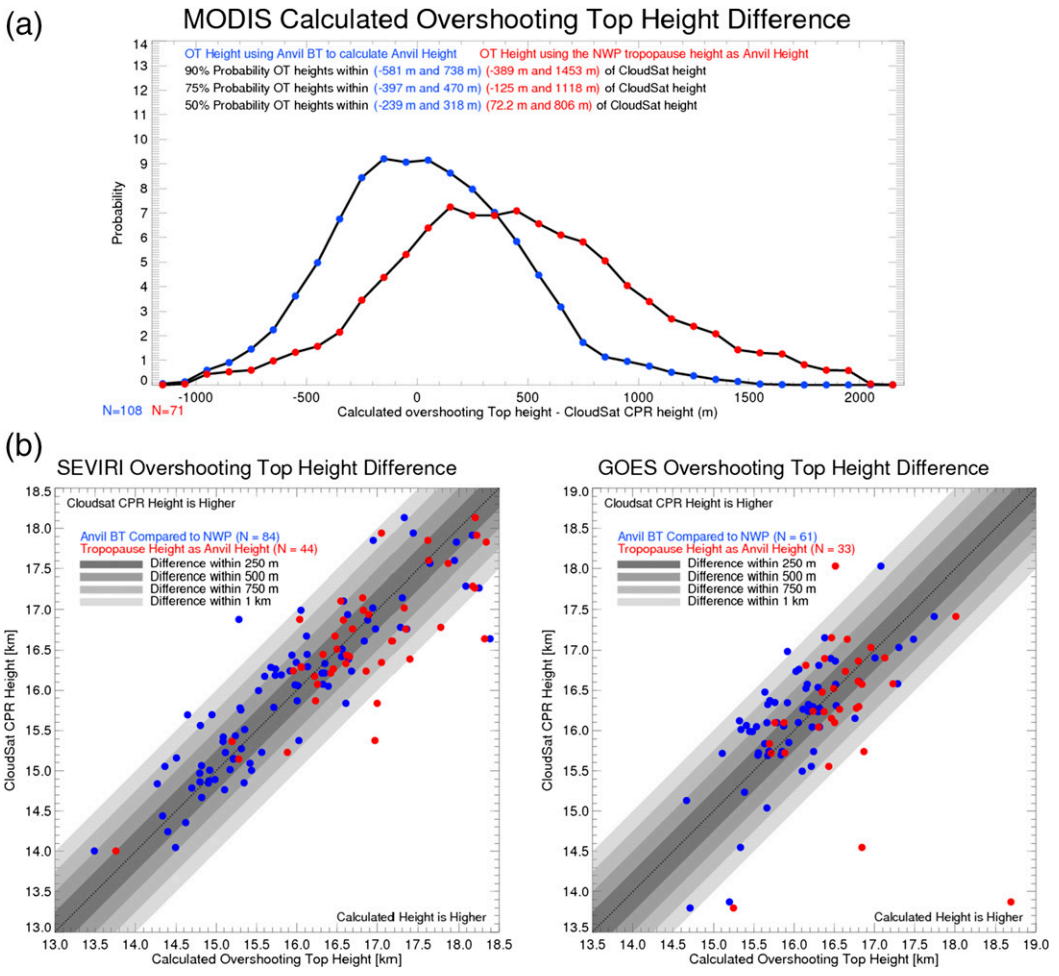

FIG. 10. (a) As in Fig. 3b (blue dots), but including the OT height calculations assuming the OT anvil height is the tropopause height (red dots). (b) Calculated overshoot height differences for the (left) SEVIRI and (right) GOES satellites. Blue (red) dots represent OT heights calculated using the anvil BT to assess the anvil height (tropopause height as anvil height). The number of OTs is reduced when utilizing the tropopause height as the OTs need to extend above the tropopause so the OT BT needs to be colder than the NWP tropopause temperature.

geopotential coordinates. However, for aviation applications, a vertical coordinate of pressure altitude is preferred (FAA 2008). Pressure altitude is defined as the altitude of a given atmospheric pressure according to the 1976 International Civil Aviation Organization (ICAO) standard atmosphere (Glickman 2000). The pressure level of the OT can be found by comparing the calculated OT height with collocated NWP height and pressure profiles.

The equation for calculating the pressure altitude depends on the geopotential pressure of the OT. The 1976 ICAO standard atmosphere tropopause is at an altitude of 11 km (Minzner 1977), or approximately 36 000 ft. According to HSD Engineering (2012), a pressure altitude of 36 000 ft is 227.9 hPa. So, for OT pressures below 227.9 hPa, the pressure altitude can be calculated using the equation

$$\text{OT Pressure Altitude} = \left[1 - \left(\frac{\text{POT}}{1013.25\,\text{hPa}}\right)^{0.190263}\right] 145\,422.16\,\text{ft}.$$

(Portland State Aerospace Society 2004), where POT is the pressure of the calculated OT height in the NWP profile. Pressure altitude for OT pressures in the stratosphere, defined as between 227.9 and 57 hPa (~65 600 ft or 20 km; Minzner 1977), can be calculated using the equation

$$\text{Overshoot Pressure Altitude} = -20\,864.238\ln(\text{POT}) + 149\,279.60\,\text{ft} \quad (6)$$

Equation (6) is the best-fit line for the data from HSD Engineering (2012), seen in Fig. 12, and has a correlation

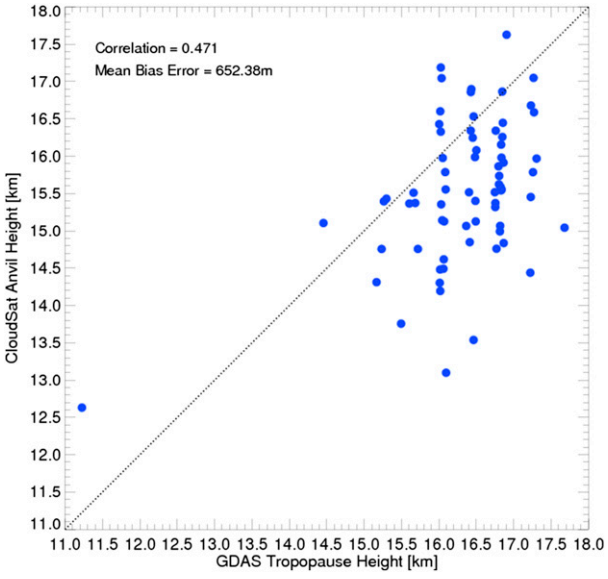

FIG. 11. The relationship between the GDAS tropopause height and the corresponding *CloudSat* anvil heights.

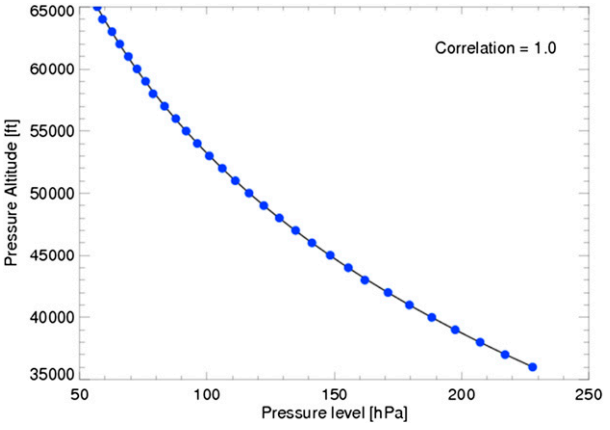

FIG. 12. The relationship between pressure level and pressure altitude from HSD Engineering (2012) for stratospheric pressures as defined by the ICAO standard atmosphere (Minzner 1977).

equal to 1.0. When comparing the calculated pressure altitude from Eq. (6) with the actual values from HSD Engineering (2012), the mean error is only 68.77 m.

6. Conclusions

This paper describes a new method for determining the height of overshooting convective cloud tops using output from an automated imager-based overshooting-top detection algorithm, the *CloudSat* Cloud Profiling Radar, and numerical weather prediction data. A set of OTs was detected using *Aqua* MODIS and geostationary satellite IR imagery and collocated with *CloudSat* CPR profiles for OT height algorithm development and validation. A lapse rate of $-7.34\,\mathrm{K\,km^{-1}}$ was determined based upon the OT–anvil BT and height differences for 108 MODIS and *CloudSat* OT events. OT heights from MODIS are calculated and compared to the CPR -25-dBZ contour (estimated cloud top from the radar). Using a cross-validation approach, it is found that 50% (75%) of MODIS-derived OT heights are within 230 m below and 340 m above (380 m below and 480 m above) the corresponding *CloudSat* height. For OTs derived from GEO satellites, 41.7% (72.6%) of the calculated OT heights from 84 SEVIRI cases are within 250 m (500 m) of the corresponding *CloudSat* height, and 37.7% (57.7%) of the calculated 61 GOES OT heights are within 250 m (500 m) of the corresponding *CloudSat* height.

OT height calculations can occasionally have differences of over 1 km when compared with the *CloudSat* heights. One potential source of these differences is the incorrect assignment of the corresponding OT anvil height. However, the method of utilizing the anvil BT to evaluate the anvil height as described in this study is more accurate than using the NWP tropopause height as a proxy for the OT anvil height.

Overall, the accuracy of the MODIS and GEO OT height assignments, coupled with the knowledge that the method presented here can provide global and near-real-time analyses of OT heights throughout the diurnal cycle with GEO data, makes it desirable for a variety of weather and climate applications. Future work on this project will include expanding the method to operate with newly available GEO satellites. Currently, relationships have been defined between MODIS-identified OTs in 1-km imagery and OTs in existing 3–4-km GEO imagers. However, new operational IR imagers on GEOs are emerging (Advanced Himawari and Baseline Imagers and the Meteosat Third Generation Flexible Combined Imager) that offer a 2-km spatial resolution. We expect the OT detection rates and fidelity of the respective height estimates to only get better as these new sensors become available.

Acknowledgments. This research was funded by GOES-R Risk Reduction Grant NA10NES4400013.

The CloudSat Cloud Profiling Radar data were obtained from the CloudSat Data Processing Center (http://www.cloudsat.cira.colostate.edu/). Satellite data were obtained from the Goddard Space Flight Center (MODIS; http://ladsweb.nascom.nasa.gov/data/) and the University of Wisconsin Space Science and Engineering Center (geostationary satellite imagery). We

thank three anonymous reviewers for very helpful inputs to improve the manuscript.

REFERENCES

Bedka, K., J. Brunner, R. Dworak, W. Feltz, J. Otkin, and T. Greenwald, 2010: Objective satellite-based detection of overshooting tops using infrared window channel brightness temperature gradients. *J. Appl. Meteor. Climatol.*, **49**, 181–202, doi:10.1175/2009JAMC2286.1.

——, R. Dworak, J. Brunner, and W. Feltz, 2012: Validation of satellite-based objective overshooting cloud-top detection methods using *CloudSat* cloud profiling radar observations. *J. Appl. Meteor. Climatol.*, **51**, 1811–1822, doi:10.1175/JAMC-D-11-0131.1.

——, C. Wang, R. Rogers, L. Carey, W. Feltz, and J. Kanak, 2015: Examining deep convective cloud evolution using total lightning, WSR-88D, and *GOES-14* super rapid scan datasets. *Wea. Forecasting*, **30**, 571–590, doi:10.1175/WAF-D-14-00062.1.

Chae, J. H., and S. C. Sherwood, 2010: Insights into cloud-top height and dynamics from the seasonal cycle of cloud-top heights observed by MISR in the west Pacific region. *J. Atmos. Sci.*, **67**, 248–261, doi:10.1175/2009JAS3099.1.

CloudSat Data Processing Center, 2007: CloudSat 2B GEOPROF quality statement: May 2007 (version R04). [Available online at http://www.cloudsat.cira.colostate.edu/sites/default/files/products/files/2B-GEOPROF_Quality-Statement.P_R04.20070501.pdf.]

Dworak, R., K. Bedka, J. Brunner, and W. Feltz, 2012: Comparison between *GOES-12* overshooting-top detections, WSR-88D radar reflectivity, and severe storm reports. *Wea. Forecasting*, **27**, 684–699, doi:10.1175/WAF-D-11-00070.1.

FAA, 2008: Principles of flight. *Pilot's Handbook of Aeronautical Knowledge*, Federal Aviation Administration, 3-1–3-10. [Available online at www.faa.gov/regulations_policies/handbooks_manuals/aviation/pilot_handbook/media/PHAK%20-%20Chapter%2003.pdf.]

Fromm, M. D., and R. Servranckx, 2003: Transport of forest fire smoke above the tropopause by supercell convection. *Geophys. Res. Lett.*, **30**, 1542, doi:10.1029/2002GL016820.

Fujita, T. T., 1972: Tornado occurrences related to overshooting cloud-top heights as determined from ATS pictures. Satellite and Mesometeorology Research Paper 97, 37 pp. [Available online at http://ntrs.nasa.gov/search.jsp?R=19730013840.]

Gettelman, A., M. L. Salby, and F. Sassi, 2002: Distribution and influence of convection in the tropical tropopause region. *J. Geophys. Res.*, **107**, 4080, doi:10.1029/2001JD001048.

Glickman, T., Ed., 2000: *Glossary of Meteorology*. 2nd ed. Amer. Meteor. Soc., 855 pp.

Goddard Earth Sciences Data and Information Services Center, cited 2015: MODIS/*Aqua*, AIRS, MLS and *CloudSat* tracks intercomparison. [Available online at disc.sci.gsfc.nasa.gov/atdd/documentation/ATrainTracks.pdf.]

Heymsfield, G. M., L. Tian, A. J. Heymsfield, L. Li, and S. Guimond, 2010: Characteristics of deep tropical and subtropical convection from nadir-viewing high-altitude airborne Doppler radar. *J. Atmos. Sci.*, **67**, 285–308, doi:10.1175/2009JAS3132.1.

Hillger, D., and Coauthors, 2013: First-light imagery from *Suomi NPP* VIIRS. *Bull. Amer. Meteor. Soc.*, **94**, 1019–1029, doi:10.1175/BAMS-D-12-00097.1.

Homeyer, C. R., and M. R. Kumjian, 2015: Microphysical characteristics of overshooting convection from polarimetric radar observations. *J. Atmos. Sci.*, **72**, 870–891, doi:10.1175/JAS-D-13-0388.1.

HSD Engineering, 2012: Altitude–pressure conversion table. [Available online at http://www.hsdengineering.com/images/ALT_PRESS_TABLE1.pdf.]

Hung, R. J., and R. E. Smith, 1982: Satellite infrared imagery, rawinsonde data, and gravity wave remote sensing of severe convective storms. *Int. J. Infrared Millimeter Waves*, **3**, 489–502, doi:10.1007/BF01007044.

Johnson, D. E., P. K. Wang, and J. M. Straka, 1994: A study of microphysical processes in the 2 August 1981 CCOPE supercell storm. *Atmos. Res.*, **33**, 93–123, doi:10.1016/0169-8095(94)90015-9.

Kaňák, J., K. Bedka, and A. Sokol, 2012: Mature convective storms and their overshooting tops over central Europe—Overshooting top height analysis for summers 2009–2011. *Extended Abstracts, 2012 EUMETSAT Meteorological Satellite Conf.*, Sopot, Poland. [Available online at http://www.eumetsat.int//website/wcm/idc/idcplg?IdcService=GET_FILE&dDocName=PDF_CONF_P61_S7_12_KANAK_V&RevisionSelectionMethod=LatestReleased&Rendition=Web.]

Kaplan, M. L., A. W. Huffman, K. M. Lux, J. J. Charney, A. J. Riordan, and Y.-L. Lin, 2005: Characterizing the severe turbulence environments associated with commercial aviation accidents. Part 1: A 44-case study synoptic observational analyses. *Meteor. Atmos. Phys.*, **88**, 129–153, doi:10.1007/s00703-004-0080-0.

Lane, T. P., R. D. Sharman, T. L. Clark, and H.-M. Hsu, 2003: An investigation of turbulence generation mechanisms above deep convection. *J. Atmos. Sci.*, **60**, 1297–1321, doi:10.1175/1520-0469(2003)60<1297:AIOTGM>2.0.CO;2.

Liu, C., and E. J. Zipser, 2005: Global distribution of convection penetrating the tropical tropopause. *J. Geophys. Res.*, **110**, D23104, doi:10.1029/2005JD006063.

——, and ——, 2008: Diurnal cycles of precipitation, clouds, and lightning in the tropics from 9 years of TRMM observations. *Geophys. Res. Lett.*, **35**, L04819, doi:10.1029/2007GL032437.

Luo, Z., G. Y. Liu, and G. L. Stephens, 2008: *CloudSat* adding new insight into tropical penetrating convection. *J. Geophys. Res.*, **35**, L19819, doi:10.1029/2008GL035330.

Mecikalski, J. R., and Coauthors, 2007: Aviation applications for satellite-based observations of cloud properties, convective initiation, in-flight icing, turbulence, and volcanic ash. *Bull. Amer. Meteor. Soc.*, **88**, 1589–1607, doi:10.1175/BAMS-88-10-1589.

Minzner, R. A., 1977: The 1976 standard atmosphere and its relationship to earlier standards. *Rev. Geophys.*, **15**, 375–384, doi:10.1029/RG015i003p00375.

Monette, S. A., C. S. Velden, K. S. Griffin, and C. M. Rozoff, 2012: Examining trends in satellite-detected tropical overshooting tops as a potential predictor of tropical cyclone rapid intensification. *J. Appl. Meteor. Climatol.*, **51**, 1917–1930, doi:10.1175/JAMC-D-11-0230.1.

NCDC, cited 2015: Global Data Assimilation System (GDAS). [Available online at https://www.ncdc.noaa.gov/data-access/model-data/model-datasets/global-data-assimilation-system-gdas.]

Pan, L. L., and Coauthors, 2014: Thunderstorms enhance tropospheric ozone by wrapping and shedding stratospheric air. *Geophys. Res. Lett.*, **41**, 7785–7790, doi:10.1002/2014GL061921.

Portland State Aerospace Society, 2004: A quick derivation relating altitude to air pressure. [Available online at psas.pdx.edu/RocketScience/PressureAltitude_Derived.pdf.]

Randall, D. A., 2009: The moist adiabatic lapse rate. [Available online at kiwi.atmos.colostate.edu/group/dave/pdf/Moist_adiabatic_lapse_rate.pdf.]

Reinke, D. L., P. T. Partain, S. P. Longmore, D. G. Reinke, and S. D. Miller, 2009: CloudSat Data Processing Center—Cloud Profiling Radar (CPR) data processing, products, and user applications. *Extended Abstracts, 34th Conf. on Radar Meteorology*, Williamsburg, VA, Amer. Meteor. Soc., 4A.2. [Available online at https://ams.confex.com/ams/pdfpapers/155251.pdf.]

Setvák, M., D. T. Lindsey, R. M. Rabin, P. K. Wang, and A. Demeterová, 2008: Indication of water vapor transport into the lower stratosphere above midlatitude convective storms: Meteosat Second Generation satellite observations and radiative transfer model simulations. *Atmos. Res.*, **89**, 170–180, doi:10.1016/j.atmosres.2007.11.031.

Sherwood, S. C., J.-H. Chae, P. Minnis, and M. McGill, 2004: Underestimation of deep convective cloud tops by thermal imagery. *J. Geophys. Res.*, **31**, L11102, doi:10.1029/2004GL019699.

Wang, C., Z. J. Luo, and Z. Huang, 2011: Parallax correction in collocating *CloudSat* and Moderate Resolution Imaging Spectroradiometer (MODIS) observations: Method and application to convection study. *J. Geophys. Res.*, **116**, D17201, doi:10.1029/2011JD016097.

Wang, P. K., M. Setvák, W. Lyons, W. Schmid, and H.-M. Lin, 2009: Further evidences of deep convective vertical transport of water vapor through the tropopause. *Atmos. Res.*, **94**, 400–408, doi:10.1016/j.atmosres.2009.06.018.

Weisz, E., J. Li, W. P. Menzel, A. K. Heidinger, B. H. Kahn, and C.- Y. Liu, 2007: Comparison of AIRS, MODIS, *CloudSat* and *CALIPSO* cloud top height retrievals. *Geophys. Res. Lett.*, **34**, L17811, doi:10.1029/2007GL030676.

Wilks, D. S., 2006: *Statistical Methods in the Atmospheric Sciences*. 2nd ed. Academic Press, 627 pp.

Wolfe, R. E., D. P. Roy, and E. Vermote, 1998: MODIS land data storage, gridding, and compositing methodology: Level 2 grid. *IEEE Trans. Geosci. Remote Sens.*, **36**, 1324–1338, doi:10.1109/36.701082.

Zipser, E. J., C. Liu, D. J. Cecil, S. W. Nesbitt, and D. P. Yorty, 2006: Where are the most intense thunderstorms on Earth? *Bull. Amer. Meteor. Soc.*, **87**, 1057–1071, doi:10.1175/BAMS-87-8-1057.